The Kinetics of Analyte Capture on Nanoscale Sensors

J. E. Solomon* and M. R. Paul†

*Condensed Matter Physics, California Institute of Technology, Pasadena, California; and †Mechanical Engineering, Virginia Polytechnic Institute and State University, Blacksburg, Virginia

ABSTRACT This article presents a number of kinetic analyses related to binding processes relevant to capture of target analyte species in nanoscale cantilever-type devices designed to detect small concentrations of biomolecules. The overall analyte capture efficiency is a crucial measure of the ultimate sensitivity of such devices, and a detailed kinetic analysis tells us how rapidly such measurements may be made. We have analyzed the capture kinetics under a variety of conditions, including the possibility of so-called surface-enhanced ligand capture. One of the modalities studied requires ligand capture through a cross-linking mechanism, and it was found that this mode may provide a robust and sensitive approach to biomolecular detection. For the two modalities studied, we find that detection of specific biomolecules down to concentration levels of 1 nM or less appear to be quite feasible for the device configurations studied.

INTRODUCTION

Over the past few years, the potential use of nanoscale electromechanical systems has been considered for high-sensitivity detection of biomolecular targets (1–3). We will refer to such devices as BioNems devices. Potential targets for such devices range from biomolecules such as proteins and enzymes, to viruses and bacteria. Since the ultimate sensitivity of such devices will depend on analyte binding efficiency, we consider a number of issues related to the kinetics of binding of biomolecular analytes to immobilized receptors (or ligands) located on a BioNems device. To provide a specific context for analysis, we consider two types of BioNems detection devices, both utilizing nanoscale cantilevers to detect the presence of bound analyte. The configurations considered here (2) are illustrated in Figs. 1 and 2. Although these devices may be used in the future for high sensitivity bioassays and measurement of binding coefficients, it is anticipated that their immediate application will be for assessing the presence or absence of specific target analytes, e.g., large proteins, enzymes, viruses, and bacteria. Thus, the analyses presented herein are in a context that is somewhat different than what is seen in typical analyses of devices such as BIAcore (Biacore Life Sciences, Uppsala, Sweden) and iASYS (iASYS, Pune, Maharashtra, India).

Fig. 1 shows a single cantilever, located within a small channel (called a ''via'') through which fluid containing the target analyte flows at some fixed velocity. Although we have chosen to consider only a single cantilever, in practice many such cantilevers can be placed in a single via to improve detection probabilities. In this configuration, binding of analyte may be detected either through mass-loading effects or through a change in the effective damping constant of the cantilever that alters the mean-square displacement of the cantilever tip. A small region at the tip of the cantilever is functionalized with immobilized receptors (or ligands) specific to the target analyte of interest. This functionalization is accomplished through the use of a self-assembling-monolayer (SAM) constructed with alkanethiols which allows linkage of analyte-specific receptors. The second device configuration is shown in Fig. 2, and is called a ''bridging configuration''. In this device, one or more cantilevers are interleaved with a single structure called a ''dock''. Both the cantilevers and dock have small regions that are functionalized for specific analytes, and detection is accomplished by the analyte binding to both cantilever and dock in a bridging fashion, as shown in Fig. 7. As discussed below, this is somewhat similar to the situation that occurs with cross-linking of cell-surface receptors by specific ligands. The bridging action of the analyte significantly changes the effective damping constant of the cantilever, and this is the effect utilized to implement analyte detection. We note that the specifics of both configurations depend to some degree on the methods of fabrication; however, Figs. 1 and 2 illustrate the essential characteristics of the two cantilever-type devices considered in this article. It should be noted that throughout this article we assume the cantilevers, in both configurations, to be immersed in a circulating fluid flow field produced by a microfluidics device; the fluid flow in this case is perpendicular to the functionalized surface. Typical linear flow velocities used in these devices are in the range of ten to several hundred microns per second, with a total fluid volume on the order of one nanoliter (B. Axelrod, BioNems Project, Caltech, private communication). This situation is in contrast with what is encountered in BIAcore-type devices (Biacore Life Sciences), where the flow field is parallel to the functionalized surface. Boundary layer effects are quite different in the two cases.

We address the analyte binding kinetics for these two device configurations under both reaction-diffusion and reaction-diffusion-convection conditions. Although steady-state solutions will yield information on maximum capture efficiency,

Submitted June 2, 2005, and accepted for publication September 26, 2005.

Address reprint requests to J. E. Solomon, Tel.: 818-395-2761; E-mail: jerry@ieyasu.compbio.caltech.edu.

0006-3495/06/03/1842/11 $2.00

doi: 10.1529/biophysj.105.067835

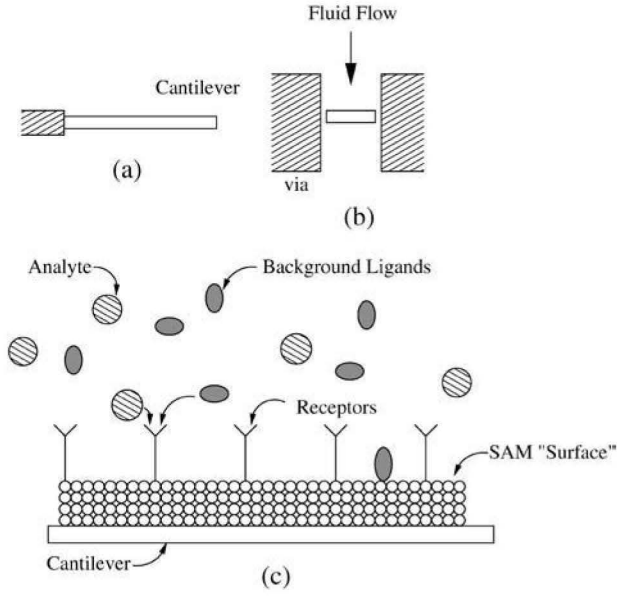

FIGURE 1 Single cantilever configuration with receptor array: (*a*) cantilever side view; (*b*) cantilever end view within via; and (*c*) analyte and background molecules seen by functionalized surface.

we also need to address the kinetics to determine the time-resolution capabilities of these systems. Under reaction-diffusion conditions, we consider both the direct binding of analyte to receptors on the SAM surface and nonspecific binding of analyte to the SAM surface followed by two-dimensional diffusion

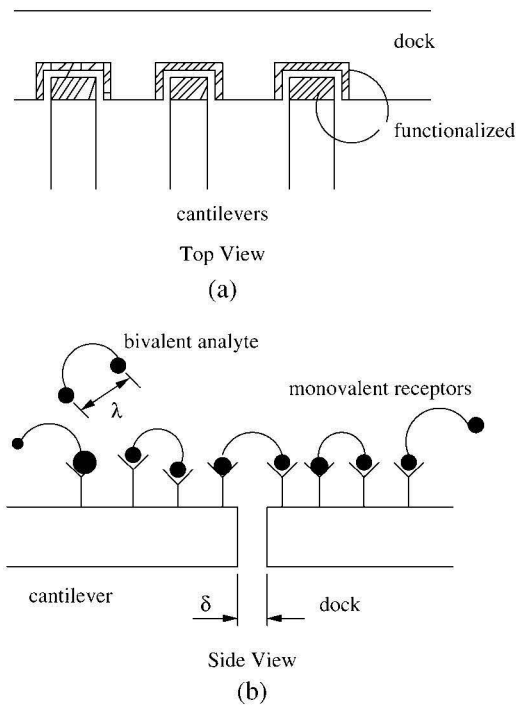

FIGURE 2 Multiple cantilever bridging configuration: (*a*) shows a top view of a multiple cantilever/dock device, and (*b*) illustrates the possible bridging modalities for ligands binding by crosslinking.

resulting in binding to a receptor. This is followed by an analysis of interference effects caused by competitive nonspecific binding of nonanalyte molecules that may be present in the system. Binding kinetics for the second (bridging) configuration is treated by a method similar to that described by Perelson and DeLisi (4) and Perelson (5), and modified for this study. Finally, we provide a discussion of analyte reaction-diffusion-convection as applied to the first device configuration. The results of this study are discussed in the final section of the article. We should also make explicit our assumption regarding the nature of analytes that may be detected by changes in the cantilever damping constant. We assume throughout that the analytes of interest are rather large, bulky proteins/enzymes, which, when attached to surface receptors, will in fact contribute to changes in the effective damping constant. Thus, we assume that small-to-medium-sized biomolecules, which constitute the majority of background contaminant, do not contribute to changes in the cantilever damping constant (discussions with members of the DARPA BioNems Project, Caltech, private communication). Finally, we emphasize that it is our intent here to provide a rather broad, but detailed, analysis of the major mechanisms affecting analyte binding kinetics; we also provide brief, but less detailed, discussions of other issues which may impact the results of the basic analysis.

Before presenting our analysis, a brief discussion of the physical parameters used in the calculations would seem to be appropriate. Without knowledge of the specific analyte-receptor pair under consideration, it is not possible to be precise in selecting values for the intrinsic forward and reverse binding coefficients. We have therefore chosen values, from among a number of pairs that have been measured (6), that are very conservative with respect to capture performance: $k_{on} = 5 \times 10^6\ M^{-1}\ s^{-1}$, and $k_{off} = 0.1\ s^{-1}$. For large-to-medium-sized biomolecules, the diffusion constant ranges from 10 to 100 $\mu^2\ s^{-1}$ (μ denotes length in microns); we have thus taken the effective bimolecular association constant, k_+, to be $10^{12}\ M^{-1}\ s^{-1}$ in the calculations below. This association rate constant is defined by $k_+ = 4\pi D_L a$, where D_L is the ligand diffusion constant, and a is a characteristic dimension of the functionalized region. Note also that the association rate constant is often denoted by k_a in the literature. We have also assumed that the cantilevers under consideration have a functionalized area at their tip of 1 μ^2, which yields a total receptor number of $\sim R_o = 10^4$ given the SAM construction methods usually employed (R. Lansford, DARPA BioNems Project, Caltech, private communication).

BASIC ANALYTE REACTION-DIFFUSION CAPTURE

Analysis of analyte binding from bulk solution to receptors immobilized on a cantilever is straightforward, and analogous to the problem of free ligand binding to cell-surface receptors (6). The process being considered may be represented by the simple reaction

$$L + R \rightleftharpoons B, \tag{1}$$

and the basic kinetic equation is given by the simple expression

$$\frac{dB}{dt} = k_f LR - k_r B, \tag{2}$$

where B is the number of ligand (analyte)-receptor bound pairs, L is the number density of ligand, R is the number of free surface-bound receptors, and the k_x values denote the forward and reverse reaction rate coefficients. However, under reaction-diffusion conditions, the forward and reverse rate constants are given by (6,7)

$$k_f = \frac{k_{on}}{1+\alpha}, \tag{3}$$

$$k_r = \frac{k_{off}}{1+\alpha}, \tag{4}$$

where we have defined $\alpha \equiv Rk_{on}/k_+$, as a reaction-diffusion index whose value indicates whether the process is reaction-limited ($\alpha \ll 1$), or diffusion-limited ($\alpha \gg 1$). Note that our treatment of α as a constant parameter is an approximation, since the value of this parameter actually decrease monotonically as the number of bound receptors increases. However, this approximation has been found to be quite good at the low analyte concentrations of interest here, and does not begin to break down significantly until the analyte concentration approaches $\approx 10^{-6}$ M. By introducing the new variables, $u \equiv B/R_o$, and $\tau \equiv k_{off}t$, we may write our kinetic equation in nondimensional form as

$$\frac{du}{d\tau} = \frac{K' - (1+K')u}{[1+\alpha(1-u)]}, \tag{5}$$

where we have introduced an additional dimensionless parameter, $K' \equiv L_o k_{on}/k_{off} = L_o K_a$. In deriving Eq. 5 we have used the conservation relation, $R = R_o - B$, and the assumption that ligand (analyte) is not significantly depleted during the course of the reaction. Since this assumption may not be strictly true under some circumstances, we discuss the ligand depletion problem later in the text.

Although Eq. 5 is nonlinear, it may be solved by a variety of numerical methods (note that we have, in all cases, utilized the ODE solvers contained in MatLab, The MathWorks, Cambridge, UK). Fig. 3 *a* illustrates solutions to Eq. 5, parameterized by α, for L_o fixed at 10^{-9} M. Fig. 3 *b* shows solutions parameterized by L_o for $\alpha = 0.05$. It can be seen from these results that as long as the process is effectively reaction-limited, useful capture efficiencies can be obtained down to analyte concentrations of 1 nM or so. In this case, a receptor binding fraction of 5% amounts to 500 bound analytes, which should be sufficient for a variety of detection methods. We consider the value $\alpha = 0.05$ to be an upper bound for virtually all conditions under which one expects these devices to be used. In some particular cases this value may be much smaller, in which case one can simply take $k_f = k_{on}$, and $k_r = k_{off}$ in the model equation.

In the above case, we chose to ignore ligand-depletion effects largely because we wish to focus on the major mechanisms that contribute to analyte capture kinetics. However, we now present a quantitative analysis of the impact of ligand depletion on ligand capture kinetics under reaction-diffusion conditions. Later, when we treat convection effects we will address this issue from a slightly different perspective. For the reaction-diffusion case, the rate equation is the same as Eq. 2, except that we now add the conservation relation

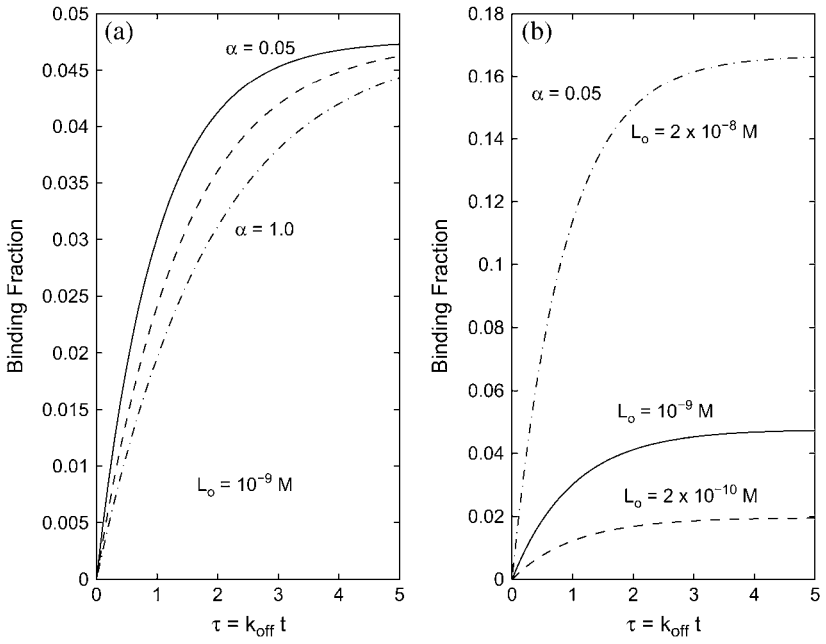

FIGURE 3 Analyte capture kinetics from bulk solution: (*a*) binding fraction parameterized by $\alpha = 0.05$, 0.1, and 1.0; and (*b*) binding fraction parameterized by ligand concentration with $\alpha = 0.05$.

$L_o = L + B$. The resulting nondimensional rate equation can be written as

$$\frac{du}{d\tau} = (1-u)(1-\lambda u)\frac{L_o}{K_d} - u, \tag{6}$$

where we define the parameter λ as

$$\lambda = \frac{n_s R_o}{N_A L_o}, \tag{7}$$

with N_A being Avogadro's number, K_d being the equilibrium dissociation constant, and n_s the number density of functionalized surfaces, or in its usual usage, the number density of cells. In a biological context, the parameter, λ, is often interpreted as a scaled cell density; one might also refer to it as a depletion index, since it measures the relative importance of ligand depletion effects. We have solved Eq. 6 for several values of λ; the resulting kinetic curves are shown in Fig. 4, *a* and *b*. These curves were computed assuming a ligand concentration of 10^{-8} M (Fig. 4 *a*), and 10^{-9} M (Fig. 4 *b*); and an equilibrium dissociation constant, K_d, of 2×10^{-8} M. An examination of these curves yields some insight into the impact of ligand depletion on the fractional occupancy of the surface receptors. In particular, we note that the receptor fractional occupancy, at fixed ligand concentration, is a nonlinear function of the depletion index. This is not particularly surprising, since the rate equation for this case is itself nonlinear. These results point up the fact that one should always check the value of the depletion index for any specific situation to determine if ligand depletion needs to be accounted for explicitly.

Another possible complicating issue for our simple model equation (Eq. 5) is the possibility of rapid rebinding of ligand to the functionalized surface immediately after release from a bound complex. Lagerholm and Thompson (8) provide a detailed analysis of this situation for the case of a membrane surface immersed in a static fluid. They develop a measure of the degree of this rebinding effect, termed the rebinding parameter, which is given by

$$b = \frac{k_f N}{k_r + k_f L_o}\sqrt{k_r/D_L}, \tag{8}$$

where we have used our notation. First, it should be noted that in virtually all instances where this effect has been seen to be significant, the solution-to-surface reaction was diffusion-limited (9). Secondly, using any particular value of this parameter to estimate the impact of rebinding on the macroscopic rate equations is very difficult, since the parameter values are unbounded on the positive real line, i.e., on the interval $[0, \infty]$. However, we note that the expression for the effective reverse reaction (dissociation) coefficient given in Eq. 4 provides a good approximation for the effects of rebinding due to diffusion of released ligand near the surface. We rewrite this equation to show the so-called reaction-diffusion index explicitly:

$$k_r = \frac{k_{off}}{1 + \dfrac{Rk_{on}}{k_+}}. \tag{9}$$

Now, Berg (10) and Goldstein and Dembo (11) have shown that, essentially, the only difference between the intrinsic dissociation rate coefficient, k_{off}, and k_r is due to rebinding effects. We may thus use our expression for k_r to estimate the actual impact of rebinding on the reaction kinetics. Thus, the fraction of dissociated ligands (analyte) that escape rebinding is given by

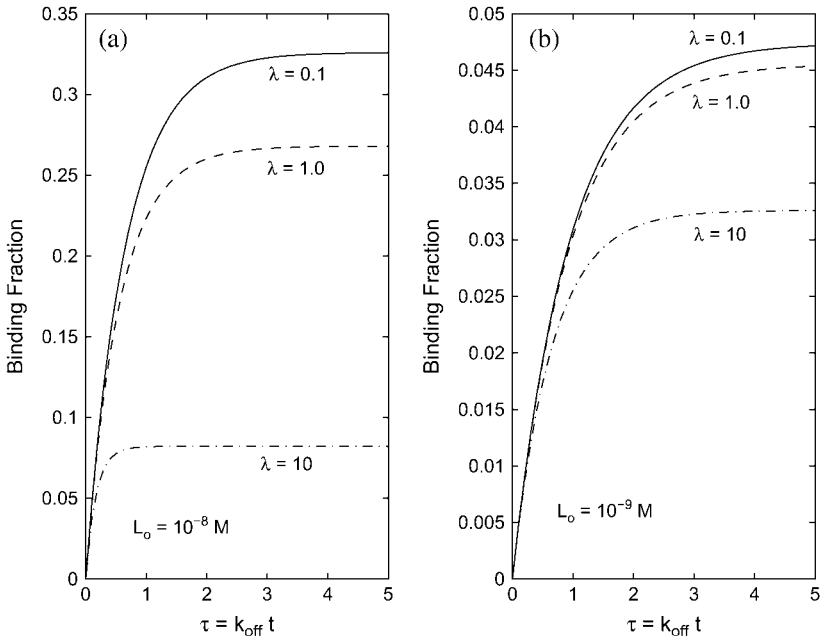

FIGURE 4 Ligand depletion effects on capture kinetics parameterized by the depletion index, λ, for two different bulk concentrations of ligand: (*a*) $L_o = 10^{-8}$ M, and (b) $L_o = 10^{-9}$ M.

$$\frac{k_r}{k_{off}} = \frac{1}{1 + \frac{Rk_{on}}{k_+}}, \tag{10}$$

and the ratio of escape to rebinding probabilities, Goldstein and Dembo (11), is given by

$$\gamma = \frac{k_+}{Rk_{on}}. \tag{11}$$

As an example, we take $R = R_o = 10^4$, $k_{on} = 5 \times 10^6\ M^{-1}\ s^{-1}$, and $k_+ = 10^{12}\ M^{-1}\ s^{-1}$, which yields 0.95 as the fraction of dissociated ligands that escape rebinding. Furthermore, the ratio of escape to rebinding probabilities is 20 for this example. It might be argued that taking $R = R_o$ is unreasonable, since R, the number of unoccupied receptors decreases during the reaction. However, we note from Fig. 3 *b* that, even under rather favorable conditions, the fraction of occupied receptors is only slightly >16% for a ligand concentration of 20 nM, and of course becomes smaller than this as ligand concentrations become smaller. Our assumption of a constant R thus appears a reasonable one. Finally we note that, under the nominal parameter values that we have assumed in this study, the value of the rebinding parameter can be in the range of ~10–50. Thus, it seems clear that even for rebinding parameter values that appear large, the actual impact of rebinding under reaction-limited conditions can be relatively small.

TWO-STEP ANALYTE BINDING

It is by now a well-established observation that, under certain conditions, the effective binding rate of a ligand from solution to a cell surface-bound receptor can be enhanced by a two-step diffusion process (6,7,11,12). This process consists of nonspecific binding of the ligand from bulk to the cell surface, followed by two-dimensional surface diffusion to a target receptor. The kinetic equations for this situation may be derived from what has been termed the "collision coupling model" (6). The purpose of this section is to investigate the specific conditions under which binding enhancement of target analytes may occur.

For the functionalized cantilever surfaces considered here, the use of SAM constructions allows one to achieve receptor densities on the order of $10^{12}\ cm^{-2}$, which is three-to-four orders-of-magnitude higher than that seen for cell surface receptors. Even at these high densities, however, much of what an analyte in solution sees is bare SAM surface unoccupied by a receptor. In fact, as much as 80%, or more, of the functionalized surface may be unoccupied by receptors in typical situations. The general situation can be seen from the illustration of the functionalized cantilever shown at the bottom of Fig. 1. For convenience in deriving the appropriate model equations we take the SAM surface to consist of discrete sites, a total of N_s, that are available to solution ligands for nonspecific binding; for this current case we take $N_s = 10^6$. We continue to take analyte-receptor binding to be a reaction-diffusion process; however, we assume that analyte-surface nonspecific binding is a reaction-limited process. This somewhat simplifies the equations, but does not materially affect our results over the range of parameters of interest in this study. This process may be written in terms of the following reaction set

$$\begin{aligned} L + S &\rightleftharpoons L_s, \\ L_s + R &\rightleftharpoons B_a, \\ L + R &\rightleftharpoons B_a, \end{aligned} \tag{12}$$

where S represents surface-binding sites and L_s represents number of surface-bound ligands. The nondimensional kinetic equations for our model may thus be written as

$$\frac{dy}{d\tau} = K_1 - K_2 y - K_3(1-u)y, \tag{13}$$

$$\frac{du}{d\tau} = \frac{K' - (1-K')u}{[1 + \alpha(1-u)]} + K_3(1-u)y, \tag{14}$$

where $y \equiv L_s/R_o$, $u \equiv B_a/R_o$, L_s is the number of surface-bound analyte, and B_a is the number of receptor-bound analyte. The nondimensional parameters are given by

$$\begin{aligned} K_1 &\equiv \frac{N_s L_o k_f^n}{R_o k_{off}}, \\ K_2 &\equiv \frac{k_r^n}{k_{off}}, \\ K_3 &\equiv \frac{R_o k_c}{k_{off}}, \end{aligned} \tag{15}$$

and K' is as before. Here, k_f^n and k_r^n are the forward and reverse rate constants for nonspecific surface binding, and k_c is the so-called collision-coupling coefficient, which defines the reaction rate for surface-bound ligand with surface-bound receptors. Although surface binding coefficients are not known with any precision, we have chosen values that would seem to be relatively conservative: $k_f^n = 10^5\ M^{-1}\ s^{-1}$, and $k_r^n = 0.1\ s^{-1}$. The collision-coupling coefficient is taken to be $k_c = 8 \times 10^{-5}\ (\#/cell)^{-1}\ s^{-1}$, as cited by Lauffenburger and Linderman (6).

Since the magnitude of this effect clearly depends on both the surface binding coefficients and the collision-coupling coefficient, we have generated two sets of solutions to our model equations. One set is parameterized by K_3, the collision-coupling coefficient, and the other set is parameterized by K_1, an effective surface binding affinity. The results are shown in Fig. 5, *a* and *b*. Note that the case of $K_3 = 0$ represents no surface enhancement, and one obtains just the usual direct ligand-receptor binding from bulk solution. Although these results show that surface-enhanced ligand-receptor binding is certainly possible, one must be cautious in making this assumption for specific cases, since the effect is very sensitive to specific parameter values.

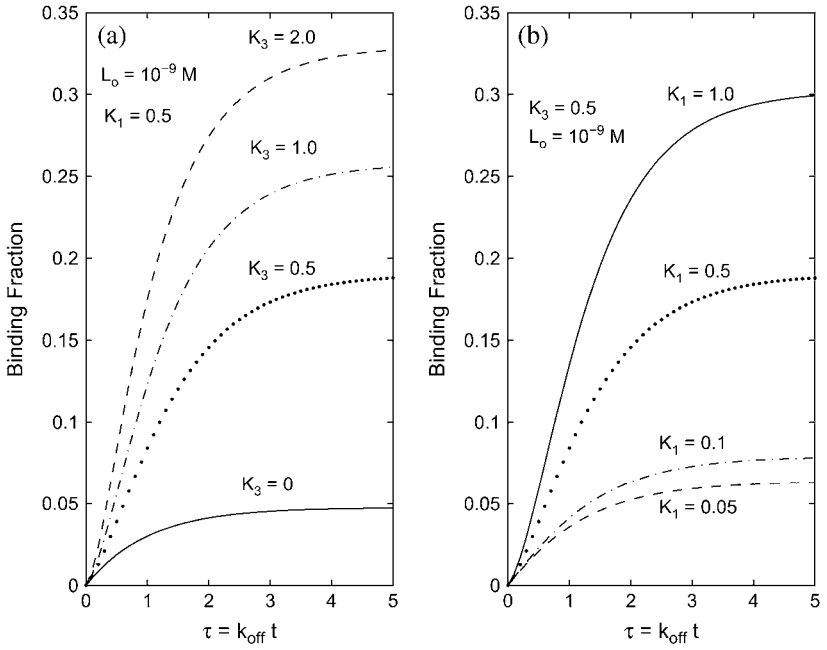

FIGURE 5 Effect of surface diffusion on analyte capture efficiency: (*a*) binding fraction parameterized by the effective collision-coupling coefficient; and (*b*) binding fraction parameterized by the effective surface binding affinity.

NONSPECIFIC BINDING BY BACKGROUND MOLECULES

It seems clear that practical BioNems devices, using a circulating solution of target analytes, will contain some level of biomolecular contaminants, and one must assess the impact of these background biomolecules on the capture efficiency of BioNems detectors. There are essentially three mechanisms by which background contaminants may affect the efficiency of analyte capture: case I, by direct competitive nonspecific binding with receptors; case II, a two-step nonspecific process similar to that described in the previous section; and case III, direct nonspecific binding of contaminant to the SAM surface. Although case II is certainly a possibility, the fact that the effective affinities involved are significantly smaller than in the case treated above makes it highly unlikely that this would be a significant mechanism in contaminant receptor binding. Since the usual sensing modality proposed for nanoscale BioNems devices relies on changes in the effective damping constant of the cantilever, case I may represent a significant interference effect. Even though the ideal situation would be one where analyte-receptor binding specificities are extremely high, this is clearly not always achievable in practice. In addition, for certain experimental measurements (e.g., detection of a specific protein/enzyme from the contents of one or more cells), some of the background biomolecules may strongly resemble the target analyte. In such cases, competitive binding of these molecules to the cantilever receptors may represent a significant effect on the analyte capture performance of the system. Case III is of importance if one is considering the use of mass-loading of the cantilever as a detection modality. Although this modality is often used with micron-scale cantilevers, such as those used in atomic force microscopy, it is probably impractical with nanoscale cantilevers. Micron-scale cantilevers can be fabricated so as to have relatively narrow mechanical resonance peaks; this allows for high resolution sensing of mass changes, but, this is generally not the case for nanoscale cantilever devices. In addition, it should be noted that this case does not represent an interference of contaminant molecules with analyte-receptor binding, since, to first-order, the surface-binding of contaminant and analyte-receptor binding are independent events. Nevertheless, for completeness, we provide a brief discussion of case III after our analysis of case I.

Case I is treated by considering the receptor-analyte binding to be a specific, high-affinity binding process, while receptor-contaminant binding is taken to be a nonspecific, low-affinity binding process. Again, the general situation can be seen from the illustration in Fig. 1 *c*. We may model this process by the following pair of nondimensional equations,

$$\frac{dy}{d\tau} = K_1 - (K_1 + K_2)y - K_1 u, \tag{16}$$

$$\frac{du}{d\tau} = K_3 - (K_3 + 1)u - K_3 y, \tag{17}$$

where our variables are $y \equiv B_c/R_o$, and $u \equiv B_a/R_o$, and B_c is the number of contaminant-bound receptors. The nondimensional parameters are given by

$$K_1 = \frac{k_f^n L_c}{k_{off}},$$

$$K_2 = \frac{k_r^n}{k_{off}},$$

$$K_3 = \frac{k_{on} L_o}{(1+\alpha)k_{off}}. \tag{18}$$

Here, L_c is the concentration of background contaminant; k_f^n and k_r^n are the forward and reverse rate constants for contaminant-receptor binding. We have taken their values to be $k_f^n = 10^5\ M^{-1}\ s^{-1}$, and $k_r^n = 0.1\ s^{-1}$.

Fig. 6 shows the relative impact of competitive binding of background contaminant for the case of $L_c = 10 \times L_o$. From these results, it seems clear that unless background contaminant levels are extremely high, competitive binding effects will not have a significant impact on the efficiency of analyte capture by the surface receptors.

We now consider an analysis of case III, which is characterized by nonspecific binding of contaminant molecules to the SAM surface. Since this process is a simple bimolecular reaction, the appropriate model equation can be written immediately as

$$\frac{dB_n}{dt} = k_f L_n (N_s - B_n) - k_r B_n, \tag{19}$$

where B_n is the number of contaminant molecules that are nonspecifically bound to the SAM surface, L_n is the concentration of background contaminant molecules, and N_s is the total number of SAM surface sites. To evaluate the magnitude of this effect we examine the steady-state solution to this equation, where we neglect ligand depletion and assume that we are in the reaction-limited regime. The result is

$$B_n = \frac{N_s}{1 + K'}, \tag{20}$$

where the parameter K' is given by $K' = K_d/L_n$, and K_d is the usual equilibrium dissociation constant. It is clear from the form of Eq. 17 that the worst-case situation is where $K' << 1$, which yields a saturation value of N_s for the number of nonspecifically bound contaminant molecules. However, even in this extreme case we note that this would result in an additional mass of the order 10^{-14} g, for a 50,000 Dalton protein, which is two orders-of-magnitude smaller than the typical total cantilever mass of $\approx 7 \times 10^{-12}$ g. Although this would represent a significant problem for the mass-loading detection modality, it would not significantly affect the detection modality considered in this article, i.e., detection by change in effective damping constant. As we noted in the Introduction, our assumption here is that target analytes of interest are large, bulky proteins/enzymes that, when bound to surface receptors, can change the cantilever damping constant. In addition, under the conditions of utilization currently expected for these devices, we assume that background contaminant will consist largely of small-to-medium-sized biomolecules that will have little or no effect on the cantilever damping constant.

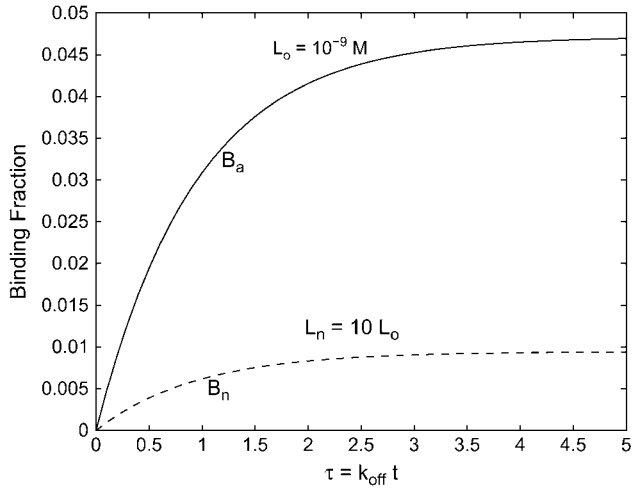

FIGURE 6 Kinetics for competitive binding of contaminant from bulk solution. The value B_a represents fraction of bound analyte, and B_n represents fraction of competitively bound contaminant.

BINDING KINETICS FOR BRIDGING MODES

A kinetic analysis of bridging mode devices, Figs. 2 and 6, is somewhat more complex; however, we have adopted an approach developed by Perelson and DeLisi (4), and Perelson (5), who analyze a similar situation with respect to cross-linking of cell-surface receptors by ligands from bulk solution. The essential difference between the cellular case and the case under consideration here lies in the geometry, not in the mechanisms. This can be seen by a consideration of Fig. 7. In this section, our notation is such that R, L, and B will always refer to the number of receptors, ligands, and bound complexes, respectively, and subscripts will be used to denote various states of these quantities (e.g., B_2 refers to a doubly-bound ligand/receptor complex).

THE MONOVALENT CASE

Given the relative binding rate coefficients for one-step versus two-step binding, it is clear that crosslinking can be modeled as a simple two-step process

$$R + L \rightleftharpoons B_1, \tag{21}$$

$$B_1 + L \rightleftharpoons B_2. \tag{22}$$

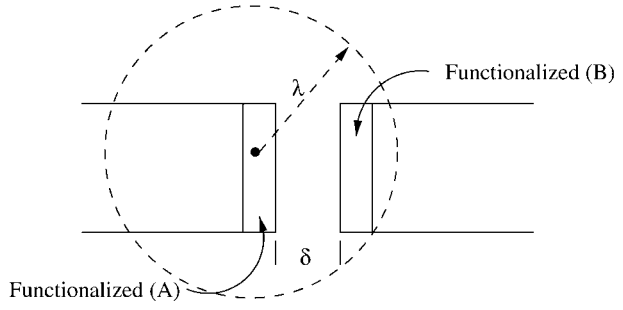

FIGURE 7 Crosslinking geometry showing the search radius of a ligand that is singly bound to a site on the cantilever, and which may make a second bond with a site on the dock.

As noted above, B_1 denotes the number of singly-bound ligands, and B_2 denotes the number of doubly-bound (crosslinked) ligands. The case we consider here is that of bivalent ligands (identical functional groups) binding with monovalent receptors uniformly distributed over a surface. The mass-action derived kinetic equations are thus

$$\frac{dB_1}{dt} = k_{1f}L_oR - k_{1r}B_1 - k_{2f}B_2 + 2k_{2r}B_2 \quad (23)$$

$$\frac{dB_2}{dt} = k_{2f}B_1R - k_{2r}B_2, \quad (24)$$

where we are using the usual notation for forward and reverse rate constants. Note that the effective rate constant for binding the free end of a singly-bound ligand, k_{2f}, is different from the rate constant for single-binding of a ligand from solution. The conservation equations for the system are

$$\begin{aligned} R_o &= R - B_1 - 2B_2 \\ L_o &= L - B_1 - B_2. \end{aligned} \quad (25)$$

Assuming ligand depletion effects to be negligible, we have

$$\frac{dB_1}{dt} = \alpha - (\beta - k_{1f}B_1)B_1 + 2(k_{2f}B_1 + k_{2r} - k_{1f}L)B_2, \quad (26)$$

$$\frac{dB_2}{dt} = k_{2f}(R_o - B_1)B_1 - 2(k_{2f}B_1 + k_{2r})B_2, \quad (27)$$

where we have defined the following parameters

$$\begin{aligned} \alpha &\equiv k_{1f}L_oR_o, \\ \beta &\equiv k_{1f}L_o + k_{2f}R_o + k_{1r}. \end{aligned} \quad (28)$$

Typical results for the monovalent case are shown in Fig. 8, where the curve labeled B_1 is for the singly-bound ligand, and the curve labeled B_2 is for the doubly bound (crosslinked) case. For this example, we have used the following parameter values: $k_{1f} = 10^8\ M^{-1}\ s^{-1}$; $k_{1r} = 100\ s^{-1}$; $k_{2f} = 8 \times 10^{-10}\ cm^2\ s^{-1}$; $k_{2r} = 1.0\ s^{-1}$; $L_o = 10^{-7}\ M^{-1}$; and $R_o = 4.25 \times 10^9\ cm^{-2}$. We should point out that these values are those appropriate for ligand cross-linking of cell surface-bound receptors (4,5). Note that, in this example, the appearance of a peak in the B_1 curve is largely due to the fact that single-binding kinetics is much faster than is the crosslinking kinetics; this behavior is not present for all choices of parameter values. Also note that "bound-fraction" refers to the ratio of number of crosslinked receptors to the total number of available receptors.

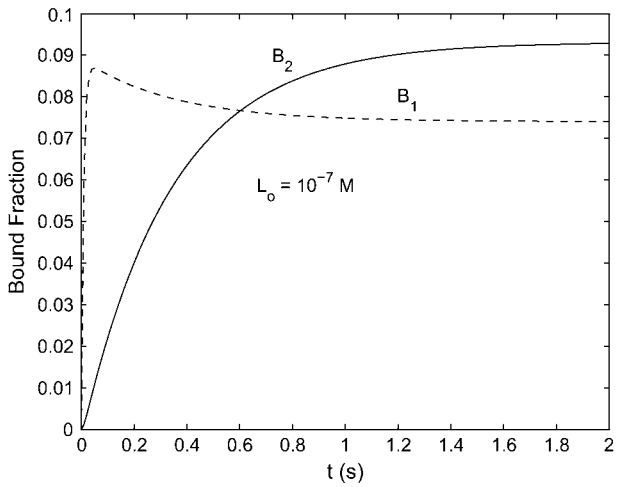

FIGURE 8 Crosslinking kinetics for homogeneous case: B_1 is the fraction of singly-bound ligand, and B_2 is the fraction of doubly-bound (crosslinked) ligand.

THE BIVALENT CASE

We now consider a case that is more appropriate for the BioNems cantilever-dock bridging configuration. We assume that the cantilevers are functionalized with a monovalent receptor, call it A, and that the dock is functionalized with a monovalent receptor denoted by B. Consequently, we consider target analytes (ligands) that are bivalent with functional groups complimentary to the two different types of receptors. Our notation for this case necessarily becomes somewhat more complicated, but is a rather straightforward extension of that used in our homogeneous case. The model kinetic equations for this situation are given by

$$\frac{dB_A}{dt} = k_f^A L_o R^A - k_r^A B_A - k_{xf}^B B_A R^B + k_{xr}^B B_{AB}, \quad (29)$$

$$\frac{dB_B}{dt} = k_f^B L_o R^B - k_r^B B_B - k_{xf}^A B_B R^A + k_{xr}^A B_{AB}, \quad (30)$$

$$\frac{dB_{AB}}{dt} = k_{xf}^B B_A R^B + k_{xf}^A B_B R^A - k_{xr}^B B_{AB} - k_{xr}^A B_{AB}, \quad (31)$$

with the conservation equations

$$\begin{aligned} R^A &= R_o^A - B_A - B_{AB}, \\ R^B &= R_o^B - B_B - B_{AB}. \end{aligned} \quad (32)$$

Note that subscripts containing an x refer to parameters related to crosslinking. Again discounting ligand depletion, typical results for solutions to these model equations are shown in Fig. 9, where the curve labeled B_A is the singly-bound A receptor, B_B is the singly-bound B receptor, and B_{AB} is for the doubly-bound (crosslinked) ligands. The parameters used in this particular example were $k_f^A = k_f^B = 10^8\ M^{-1}\ s^{-1}$; $k_r^A = 10\ s^{-1}$; $k_r^B = 20\ s^{-1}$; $k_{xf}^A = k_{xf}^B = 8 \times 10^{-10}\ cm^2\ s^{-1}$; $k_{xr}^A = 1.0\ s^{-1}$; $k_{xr}^B = 2.0\ s^{-1}$; $R_o^A = R_o^B = 4.25 \times 10^9\ cm^{-2}$; and $L_o = 10^{-7}$ M. Again, we have used parameters suitable for the case of ligand cross-linking of cell surface-bound receptors. We next examine the situation that pertains directly to the bridging configuration.

Since detection of a bridging event requires specific crosslinking between a cantilever and its docking space, we choose to use the bivalent ligand case treated above to model the capture kinetics for this configuration. This is due to the fact that monovalent ligands can crosslink on a cantilever alone and on the docking area alone, without forming a

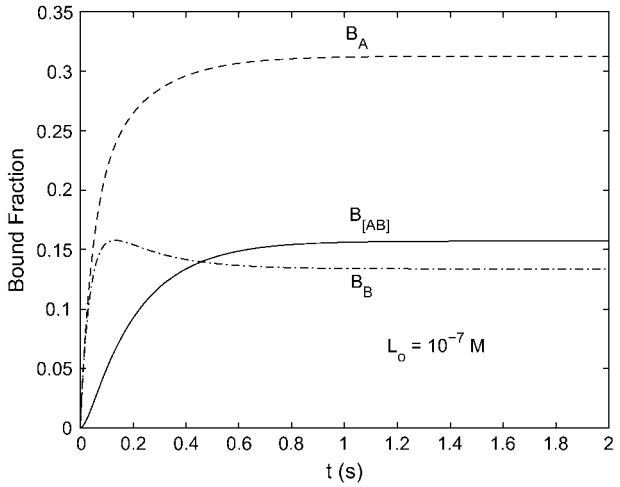

FIGURE 9 Crosslinking kinetics for heterogeneous case: B_A is the fraction of singly-bound A-ligand, B_B is the fraction of singly-bound B-ligand, and $B_{[AB]}$ is the fraction of doubly-bound (crosslinked) ligand.

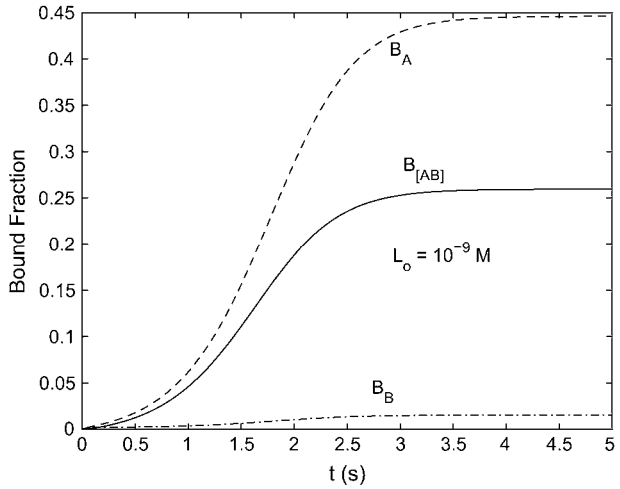

FIGURE 10 Bridging device with $\gamma = 0.005$: B_A is the fraction of singly-bound A-analyte, B_B is the fraction of singly-bound B-analyte, and $B_{[AB]}$ is the fraction of doubly-bound (crosslinked) analyte.

cantilever-dock bridge; this makes for rather inefficient capture from a detection standpoint. In the usual biology crosslinking problem, the receptors, R^A and R^B, are assumed to be uniformly distributed over a single cell surface; and these are the conditions under which the crosslinking rate constants are usually measured (4–6). However, our bridging problem is somewhat different, since the two receptor types are physically separated (refer to Fig. 7). Without rewriting our model equations to explicitly account for this physical separation, we make the approximation that, to first-order, the effect of spatial separation is a reduction in the effective crosslinking rate-constant due to geometric effects alone. Denoting by A_d the functionalized area on the dock, and by A_s the search area for a singly-bound ligand, then it is clear that we must reduce the effective crosslinking rate constant by (at least) a factor of $\gamma = A_d/A_s$. In addition, we note that receptor densities achievable using SAM structures are several orders-of-magnitude higher than the usual receptor densities observed on cell surfaces. Typical densities using SAM fabrications are of the order of 10^{12} cm^{-2}. Using this value for $R_o^A = R_o^B$, and taking $L_o = 10^{-9}$ M, while keeping the other parameter values the same, Figs. 10 and 11 show crosslinking kinetics for $\gamma = 0.005$ and $\gamma = 0.01$, respectively.

Despite the rather drastic reduction in the cross-linking rate constant, and ligand concentration, these results show that detection of analyte through cross-linking between cantilever and dock may be a feasible means of detection. However, a word of caution regarding the behavior of the model equations used is in order. Although we have not carried out a formal stability analysis of these equations, we have found empirically that the system exhibits incipient instabilities for specific choices of k_{xf}^i and k_f^i. Given the nature of this coupled nonlinear system, such a result is, of course, not surprising.

THE CONVECTION PROBLEM

We have assumed that the cantilever systems considered in the above analyses are incorporated into a microfluidics device that provides a steady fluid flow over the cantilever. Thus, we need to examine the possible effects of this flow field on the analyte capture kinetics. To examine the nature of this flow field, consider Fig. 1 *b* with a z axis (positive in the upward direction) drawn through the center of the cantilever; and an x axis (perpendicular to the z axis) drawn coincident with the cantilever surface. Using these coordinates, we may describe the fluid flow near the cantilever surface as a two-dimensional viscous stagnation-point flow, whose velocity components are given by (13)

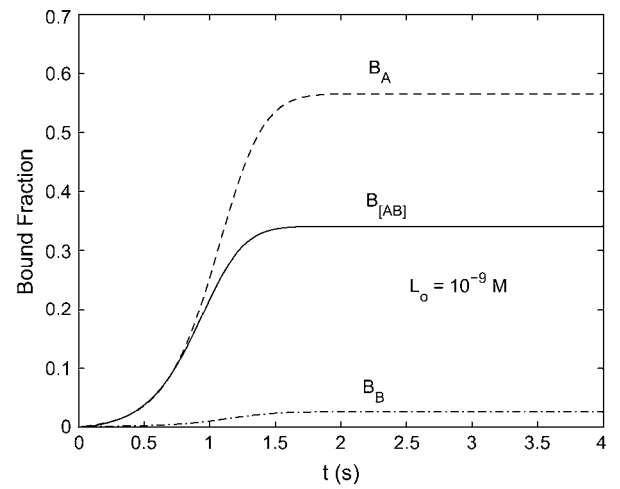

FIGURE 11 Bridging device with $\gamma = 0.01$; notation is the same as in Fig. 10.

$$U_x = Gxz, \quad U_z = -Gz^2. \tag{33}$$

Here the factor, G, is proportional to the fluid flow velocity, and U_o, above the stagnation field. A rather complete analysis of surface reactions under conditions of stagnation-point flow has been given by Edwards (14). Although his analysis assumes high-Reynolds-number potential flow, the actual Reynolds number for his system was ~300, and the flow was still in the laminar regime. The analysis by Edwards matches a potential flow to a stagnation point flow near the surface. Although the conditions under which nanoscale cantilevers operate are low-Reynolds-number viscous flow, the stagnation point flow analysis coupled to the diffusion-reaction equations is still relevant to our situation.

A complete analysis of this problem requires solving the convection-diffusion transport equations with the ligand-receptor reaction at the surface providing a boundary condition. However, for our purpose, we follow Edwards' observation that the critical dimensionless parameter for this problem is the Damkohler number, Da, which may be written as

$$Da = \frac{k_{on} R_d \delta}{D_L}, \tag{34}$$

where R_d is the receptor surface density, and δ is the effective thickness of the diffusion boundary layer. This parameter essentially measures the ratio of the reaction velocity to the diffusion velocity within the boundary layer at the cantilever surface. Note also that the thickness of the stagnation flow region is generally much greater than the diffusion boundary layer thickness (14,15). Converting k_{on} to appropriate units (cm^3 $molecule^{-1}$ s^{-1}), and using the approximate expression for the diffusion boundary layer thickness (16),

$$\delta \approx a(1/Pe)^{1/3}, \tag{35}$$

with Pe, the Peclet number, defined by aU_o/D_L, and a being a characteristic length (in our case the cantilever width), we find that the value of Da is ~0.05–1.0 for the range of parameters used in this analysis.

As Edwards (14) notes, the effect of small Damkohler numbers on the reaction-diffusion-convection equations is that the reaction velocity is slow enough that there is little drain on the total flux delivered to the capture surface. Under these conditions, the effective ligand concentration near the cantilever surface remains close to the bulk concentration. This constitutes our second reason for neglecting ligand depletion in the kinetic analyses presented earlier. However, we must point out that as Da approaches unity, diffusion-convection effects become more important. The general result of this is that the effective ligand concentration at the cantilever surface can become significantly less than L_o. Thus, for operating parameters that result in Da becoming greater than unity, one must generally solve the complete reaction-diffusion-convection problem to obtain good estimates of the analyte capture efficiency for these systems. Such a detailed analysis is clearly beyond the scope of this article, though it provides an interesting problem for future work.

DISCUSSION

We have presented a rather broad, but detailed analysis of the major mechanisms driving analyte capture kinetics for two specific nanoscale cantilever devices. In addition, we have provided less detailed discussions of several issues that can affect the results of our broader analysis, and attempted to point out how they may be addressed. We have not attempted to describe or analyze specific methods for detection, or provide estimates of actual performance of these devices since that is clearly a subject for another article. We should note, however, that there are two basic sensing modalities used with the type of devices considered in this article: 1), changes in cantilever mass due to mass-loading effects of analyte capture; and 2), changes in the effective cantilever damping coefficient, $\gamma_e(\rightarrow \gamma'_e)$, due to the attachment of relatively large, bulky biomolecular analytes. Relatively high sensitivities to cantilever mass changes can be achieved for micron-scale cantilevers using, e.g., phase-controlled feedback methods (17,18) in various media. Achieving high sensitivities with a cantilever system immersed in liquid is, however, very difficult; this is particularly true of nanoscale devices. The reason for this is simply that detection-of-mass changes requires sensing cantilever vibrational frequency changes with high resolution, i.e., one needs a system with relatively high Q. In addition, as noted earlier, background contaminant molecules entrained in the circulating may contribute significantly to mass-loading depending on their concentration and their nonspecific binding affinities for the SAM surface. Thus, sensing modality (see 1, above) is not generally the modality of choice for the devices considered here.

Sensing modality (see 2, above) relies on detecting changes in γ_e caused by analyte binding to the cantilever. It is straightforward to show, using the fluctuation-dissipation theorem, that the fundamental signal/noise ratio for this modality will be proportional to γ'_e/γ_e. In this case the presence of analyte is detected by changes in the mean-square fluctuations of the cantilever tip. Thus, this modality is less sensitive to the effects of mass-loading by contaminants, and does not require a high Q system.

In terms of capture efficiency, our results for single functionalized cantilevers would seem to indicate that detection of biomolecules down to the level of 1 nM or less should be feasible. The question of surface-diffusion enhancement of analyte capture was explored, and quantitative results indicate that this mechanism might prove advantageous to increasing analyte capture efficiency under certain circumstances—although, clearly, this will depend on the particular parameters that characterize a specific device implementation. In light of the discussion above regarding sensing modalities, a full sensor sensitivity evaluation must combine the analyte capture efficiency results with the expected (per analyte) change in γ_e.

The cantilever-dock bridging configuration that was analyzed presents some interesting possibilities for robust and sensitive detection of a certain class of analytes, i.e., ligands possessing bivalent active groups. At least for the parameters used in this study, the analyte capture efficiency appears to be quite good. However, given that the class of ligands useful in this mode is very restricted, it may be that this device configuration would be better applied to detecting target analytes that consist of relatively short DNA oligomers, with the cantilever and dock being functionalized with the appropriate DNA strands complimentary to the two ends of the oligomer. In this case, of course, the capture efficiency will depend on the specific hybridization rates for the species used.

We have also addressed the issue of convection in BioNems cantilever type devices since most proposals for their use involve incorporation into microfluidics systems to maintain a constant flow of analyte. Relatively simple fluid dynamics arguments were used to show that, at the bulk flow velocities useable in such devices, and for system Damkohler numbers less than unity, capture efficiencies are likely to be dominated by reaction-diffusion mechanisms. In these cases convection is unlikely to play a significant role in analyte capture efficiencies. However, we also noted that for $Da \geq 1$, one must generally solve the coupled convection-diffusion-reaction equations to obtain an accurate picture of analyte binding kinetics, and thus capture efficiencies. Although such an analysis is beyond the scope of this article, it provides a challenging problem for future work. Finally, we note that at analyte concentrations below ~ 1 nM, stochastic effects will become important in analyzing the detection behavior of these devices, i.e., fluctuations will become an important factor. We are currently developing methods to analyze this case using a technique based on the stochastic simulation algorithm of Gillespie (19,20).

The authors gratefully acknowledge numerous useful discussions with various members of this project. We also thank one of the reviewers for several stimulating comments on some important issues related to the analyses presented in this article.

This work was partially supported by the Caltech BioNems project (M. L. Roukes, Principal Investigator), funded by Defense Advanced Research Projects Agency Simbiosys under grant No. F49620-02-1-0085.

REFERENCES

1. Roukes, M., S. Fraser, M. Cross, and J. Solomon. 2000. U.S. Patent App. No. 60/224:109.
2. Ekinci, K. L., and M. L. Roukes. 2005. Nanoelectrical systems. *Rev. Sci. Instrum.* 76:1–12.
3. Paul, M. R., and M. C. Cross. 2004. Stochastic dynamics of nanoscale mechanical oscillators immersed in a viscous fluid. *Phys. Rev. Lett.* 92: 235501–1–235501–4.
4. Perelson, A. S., and C. DeLisi. 1980. Receptor clustering on a cell surface. I. Theory of receptor cross-linking by ligands bearing two chemically identical functional groups. *Math. Biosci.* 48:71–110.
5. Perelson, A. S. 1980. Receptor clustering on a cell surface. II. Theory of cross-linking by ligands bearing two chemically distinct functional groups. *Math. Biosci.* 49:87–110.
6. Lauffenburger, D. A., and J. J. Linderman. 1993. Receptors. Oxford University Press, New York.
7. Adam, G., and M. Delbruck. 1968. Structural Chemistry and Molecular Biology. A. Rich and N. Davidson. Freeman, San Francisco, CA.
8. Lagerholm, B. C., and N. L. Thompson. 1998. Theory for ligand rebinding at cell membrane surfaces. *Biophys. J.* 74:1215–1228.
9. Geurts, B. J. 1989. Diffusion-limited immunochemical sensing. *Bull. Math. Biol.* 51:359–379.
10. Berg, O. G. 1978. On diffusion-controlled dissociation. *Chem. Phys.* 31:47–57.
11. Goldstein, B., and M. Dembo. 1995. Approximating the effects of diffusion on reversible reactions at the cell surface: ligand-receptor kinetics. *Biophys. J.* 68:1222–1230.
12. Berg, O. G. 1985. Orientation constraints in diffusion-limited macromolecular associations: the role of surface diffusion as rate-enhancing mechanism. *Biophys. J.* 47:1–15.
13. Pozrikidis, C. 1997. Introduction to Theoretical and Computational Fluid Dynamics. Oxford University Press, New York.
14. Edwards, D. A. 2000. Surface reaction near a stagnation point. *Studies Appl. Math.* 105:1–29.
15. Milne-Thomson, L. M. 1996. Theoretical Hydrodynamics, Ch. 23. Dover Publications, Mineola, NY.
16. Russel, W. B., D. A. Saville, and W. R. Schowalter. 1999. Colloidal Dispersions. Cambridge University Press, Cambridge, UK.
17. Durig, U., H. R. Steinauer, and N. Blanc. 1997. Dynamic force microscopy by means of the phase-controlled oscillator method. *J. Appl. Phys.* 82:3641–3651.
18. Tamayo, J., A. D. L. Humphris, R. J. Owen, and M. J. Miles. 2001. High-Q dynamic force microscopy in liquid and its application to living cells. *Biophys. J.* 81:526–537.
19. Gillespie, D. T. 1976. A general method for numerically simulation the stochastic time evolution of coupled chemical reactions. *J. Comput. Phys.* 22:403–434.
20. Gillespie, D. T. 1977. Exact stochastic simulation of coupled chemical reactions. *J. Phys. Chem.* 81:2340–2361.